iScience

CellPress
OPEN ACCESS

Article

Tuning the Binding Affinity of Heme-Responsive Biosensor for Precise and Dynamic Pathway Regulation

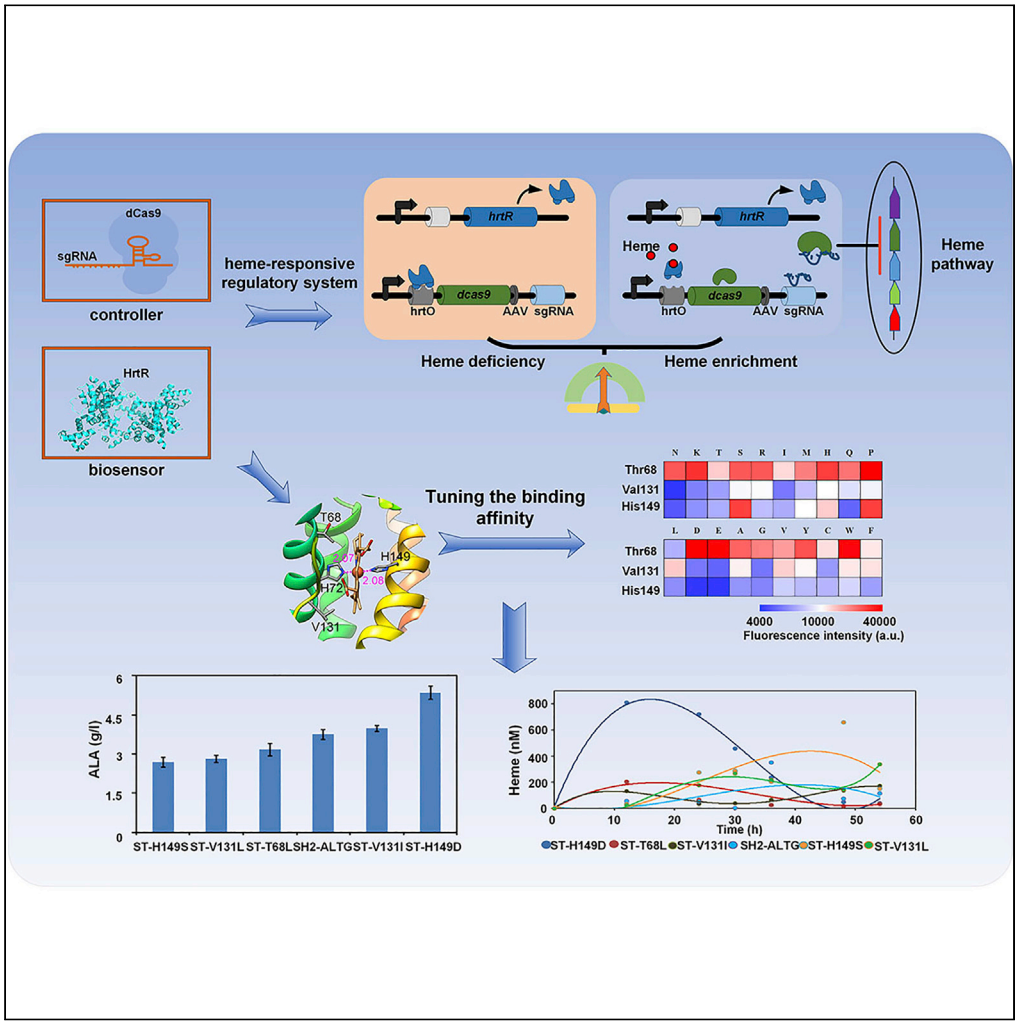

Jian Zhang, Zhiguo Wang, Tianyuan Su, Huanhuan Sun, Yuan Zhu, Qingsheng Qi, Qian Wang

qiqingsheng@sdu.edu.cn (Q.Q.)
qiqi20011983@gmail.com (Q.W.)

HIGHLIGHTS

Designed and built a heme-responsive regulatory system employing HrtR and CRISPRi

Turning the binding affinity of HrtR by site saturation mutations

Optimizing the system to achieve dynamic regulation of target genes

The system was applied to the ALA, PBG, and porphyrins production

Zhang et al., iScience 23, 101067
May 22, 2020
https://doi.org/10.1016/j.isci.2020.101067

iScience

CellPress
OPEN ACCESS

Article

Tuning the Binding Affinity of Heme-Responsive Biosensor for Precise and Dynamic Pathway Regulation

Jian Zhang,[1] Zhiguo Wang,[2] Tianyuan Su,[1] Huanhuan Sun,[1] Yuan Zhu,[1] Qingsheng Qi,[1,3,*] and Qian Wang[1,4,*]

SUMMARY

Current challenge for dynamic pathway control in metabolic engineering is enabling the components of the artificial regulatory system to be tunable. Here, we designed and built a heme-responsive regulatory system containing a heme biosensor HrtR and CRISPRi to regulate chemicals production while maintaining the intracellular heme homeostasis. A series of engineered biosensors with varied sensitivity and threshold were obtained by semi-rational design with site saturated mutation of HrtR. The modified metabolite-binding affinity of HrtR was confirmed by heme titration and molecular dynamic simulation. Dynamic regulation pattern of the system was validated by the fluctuation of gene expression and intracellular heme concentration. The efficiency of this regulatory system was proved by improving the 5-aminolevulinic acid (ALA) production to 5.35g/L, the highest yield in batch fermentation of *Escherichia coli*. This system was also successfully used in improving porphobilinogen (PBG) and porphyrins biosynthesis and can be applied in many other biological processes.

INTRODUCTION

Traditional microbial production of valuable chemicals mainly involves constitutive or inducible expression of pathway enzymes under static control, which imposes burden and even generates suboptimal growth caused by imbalanced cofactors or toxic intermediates accumulation (Glick, 1995; Martin et al., 2003). In comparison, natural cells maintain robust growth and withstand environmental fluctuations by dynamically adjusting cellular metabolism through complex regulatory networks (Shen-Orr et al., 2002). Thus, "dynamic control" of metabolic pathway would reinforce hosts robustness and high production yield.

A synthetic dynamic control system/circuit typically consists of a biosensor and a genetic controller. Biosensor is a key component of dynamic regulatory system, which is metabolites responsive and should provide desired input-output relationships. Therefore, the tunability of the biosensor is of great importance; it must respond to a certain range of metabolites concentration with the appropriate sensitivity and threshold to ensure the precise regulation of host metabolism. The application of biosensors and genetic control circuits in metabolic engineering has been extensively reviewed (Brophy and Voigt, 2014; Liu et al., 2015a; Mahr and Frunzke, 2016). So far, many biosensor-based regulatory circuits have been built, whereas a few pioneering studies (Liu et al., 2015b; Xu et al., 2014; Zhang et al., 2012) can actually realize the detected dynamic regulation and can prove the existence of metabolite fluctuation. Several reports have demonstrated that tuning the biosensor performance can increase production (Liu et al., 2015b; Xu et al., 2014). However, these studies mainly focus on TF expression level, such as plasmid copy number, number of TF binding sites (Trabelsi et al., 2018) and promoter engineering (Mannan et al., 2017) (Blazeck and Alper, 2013; Feng et al., 2018). Few studies reported the alteration of the sensitivity and threshold of the biosensor through the modification of the ligand-binding affinity (Taylor et al., 2016).

Heme is a critical biological macromolecule that serves as a redox active prosthetic group required for many cellular processes, such as respiration, cellular differentiation, signal transduction, circadian rhythm pathways, and gas sensing (Bonyhady et al., 1982; Chen and London, 1981; Shelver et al., 1997). Therefore, heme is necessary for cells to maintain normal physiological functions (Tsiftsoglou et al., 2006). However, excessive free heme (>1 μM) is toxic to cells (Ryter and Tyrrell, 2000). In *Escherichia coli*, the biosynthesis of heme involves the formation of 5-aminolevulinic acid (ALA) as a precursor (Layer et al., 2010) and

[1]State Key Laboratory of Microbial Technology, National Glycoengineering Research Center, Shandong University, Qingdao 266237, P. R. China

[2]Institute of Ageing Research, School of Medicine, Hangzhou Normal University, Hangzhou 311121, P. R. China

[3]CAS Key Lab of Biobased Materials, Qingdao Institute of Bioenergy and Bioprocess Technology, Chinese Academy of Sciences, Qingdao 266101, P. R. China

[4]Lead Contact

*Correspondence: qiqingsheng@sdu.edu.cn (Q.Q.), qiqi20011983@gmail.com (Q.W.)

https://doi.org/10.1016/j.isci.2020.101067

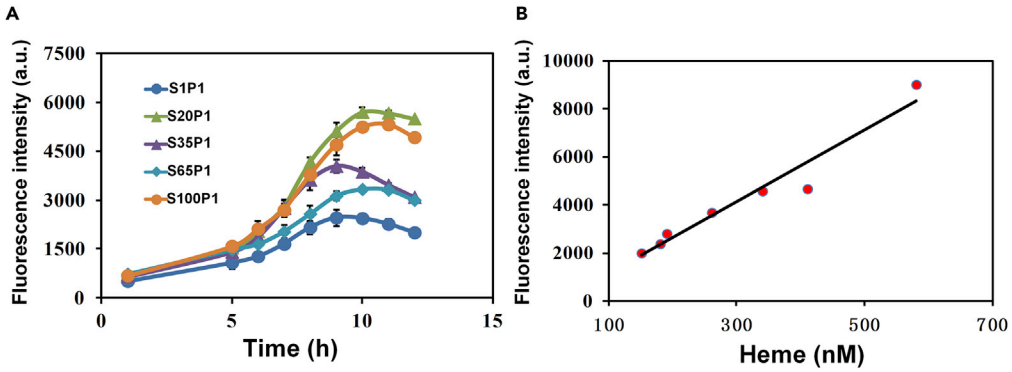

Figure 1. The Evaluation the Relationship of Fluorescence Intensity and Intracellular Free Heme Concentration of the Heme Responsive Biosensor

(A) The GFP expression intensity of *E. coli* strains S1P1, S20P1, S35P1, S65P1, and S100P1.

(B) Linear relationship between green fluorescence intensity and intercellular heme concentration. Error bars represent ±1 SD from the mean of three replicate cultures.

subsequent condensation of two ALA molecules into porphobilinogen (PBG), which finally generates heme via porphyrins (Choby and Skaar, 2016). The indispensability and toxicity of heme raises the difficulties in engineering the metabolic pathway related to heme biosynthesis, such as ALA, vitamin B12, siroheme, and chlorophyll. Therefore, it is essential to develop a regulatory system to enhance metabolic flux while still maintaining *in vivo* heme homeostasis.

Here, we designed and constructed a heme-responsive regulatory system to control the metabolic pathway dynamically and precisely. HrtR, a heme-sensing transporter regulator from *Lactococcus lactis* (Sawai et al., 2012), was used as the biosensor and CRISPR interference (CRISPRi) (Fontana et al., 2018; Qi et al., 2013) as a controller. This synthetic regulatory system was optimized with regard to its sensing and controlling components and was applied to pathway engineering.

RESULTS

Design and Characterization of a Heme-Responsive Biosensor

Organism has evolved sophisticated heme regulatory system to maintain *in vivo* heme at a reasonable level via heme-sensing proteins (Frunzke et al., 2011). These proteins bind heme reversibly (Baureder and Hederstedt, 2013) and are usually not conserved in prokaryotic (Qi et al., 1999) and eukaryotic cells (Ding et al., 1994; Han et al., 2007). HrtR acts as a heme-sensing repressor for the regulation of heme-efflux system through hrtRBA operon in *Lactococcus lactis* (Sawai et al., 2012), binds to a 15-nt special DNA sequence (*hrtO*) located in the promoter region, and controls heme homeostasis by sensing intracellular heme (Lechardeur et al., 2012). Therefore, HrtR and *hrtO* were selected for a heme-responsive biosensor in this study.

To evaluate the heme-responsive biosensor, the *hrtO*-hybrid trc promoter was placed upstream of *gfp* under the control of HrtR, resulting in plasmid P1. A recombinant *E. coli* strain containing different copy numbers of glutamyl-tRNA reductase gene (*hemA*) and glutamate-1-semialdehyde aminotransferase gene (*hemL*) on the genome was employed to achieve different intracellular heme accumulation (Cui et al., 2019). Strains S1, S20, S35, S65, and S100 represented 1, 20, 35, 65, and 100 copies of *hemA*/*hemL* integrated on the genome. The above five strains were obtained through chemically inducible chromosomal evolution (CIChE) method previously in our laboratory (Tyo et al., 2009). Then plasmid P1 was transformed into recombinant *E. coli* strains. The fluorescence intensity in these strains was gradually enhanced with the increased *hemA*/*hemL* copy numbers (Figure 1A). To investigate the correlation between heme and fluorescence intensity, the intracellular heme concentration and green fluorescence intensity were also measured and analyzed. As shown in Figure 1B, the fluorescence intensity was positively correlated with intracellular heme concentration and proved that HrtR can be used as a heme-responsive biosensor.

Semi-Rational Design of Heme-Responsive Biosensor with Varied Binding Affinity

Biosensor with tailor-made ligand-binding affinity is the prerequisite for precise regulation. Heme interacts with HrtR through two histidines, His-72 and His-149, coordinates to the heme iron. The coordination

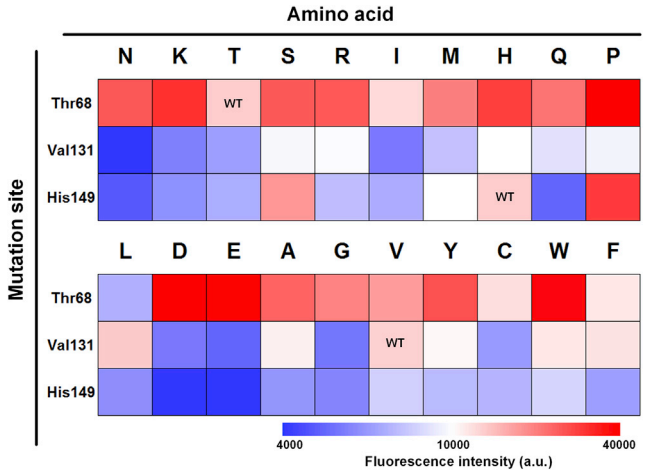

Figure 2. The GFP Expression Intensity Heatmaps of Promoters Regulated by HrtR Saturation Mutant Library
Experimental data are available in Table S1.

between Histidines 72 and 149 with heme was supposed to form a strong affinity between HrtR and heme (Sawai et al., 2012). *In vitro* experiments showed that the addition of 1 μM heme was sufficient to fully dissociate HrtR from DNA. Based on the crystal structure of holo HrtR (PDB : 3VP5), three residues including H149 that form coordinate bond with Fe atom, V131 that locates at the entrance loop (P125-G135) of heme binding cavity, and the polar residue T68 that locates close to the nonpolar part of heme porphyrin were selected and were performed saturated mutation. The mutants were found to affect the binding affinity dramatically, which was reflected in the variation of fluorescence from 32.4% up to 280.5% of the wild-type (Figure 2, Table S1). Among the 19 mutants at the T68 site, most had higher fluorescence intensity than the wild-type except mutant T68L. On the contrary, mutations at the V131 site caused an obvious decrease in fluorescence intensity except V131L. Remarkably, the alteration of the coordination bond had a significant effect on the fluorescence intensity. Compared with the wild-type, the H149D and H149E reduced the fluorescence intensity by approximately 67%, whereas the H149S and H149P increased the fluorescence intensity by approximately 122%. Since protein engineering at key sites of heme binding changed biosensor's output effectively (Figure 3B), a precise calibration of the biosensor was carried out.

To characterize the function of constructed heme-responsive biosensors, the dose-response curves of the wild-type and five chosen mutants, H149D, H149S, V131L, V131I, and T68L, were determined. Since *E. coli* K-12 strains have no natural heme uptake system, heme transporters from three different origins were selected to express in *E. coli* DH5α, such as HasA/R from *Serratia marcescens* and HutA from *Bartonella*. Only ChuA from *E. coli* O157:H7 EDL933 was effective. We established a dose-response relationship of heme and the GFP output expression of the biosensors in the ChuA-expressing strain. The fluorescence intensity was measured after cultivation for 8 h with different heme concentrations (0.01–20 μM). Since the addition of heme will affect the measurement of fluorescence, the maximum concentration added is set as 20 μM. The results are shown in Figure 3C. HrtR and its mutants H149S, T68L, and V131L showed standard dose-response curves. But 20 μM heme is not enough to support complete dissociation of mutants H149D and V131I. In addition to H149D and V131I, the dynamic range, sensitivity, and EC_{50} of the other biosensors were all calculated (Figure 3E). Compared with the wild-type, the dynamic ranges of the mutants were slightly reduced and the sensitivities of T68L and V131L to heme was significantly reduced. The EC_{50} of the different mutants in ascending order was H149S, WT, T68L, V131L.

To verify the heme responses of H149D and V131I, the *in vitro* heme affinity of HrtR and the five mutants was detected by titrating heme into apo-HrtR and measuring the change in absorbance at 413 nm (Figure 3D) (Sawai et al., 2012). When the molar ratio of heme to protein reached 1.5, H149S first reached saturation. As the ratio increased, other mutants became saturated in turn. This indicates that the heme affinity of H149D and V131I was less than that of other mutants. Figures 3D and 3E together showed that the descending order of affinity to heme is H149S, WT, T68L, V131L, V131I, H149D.

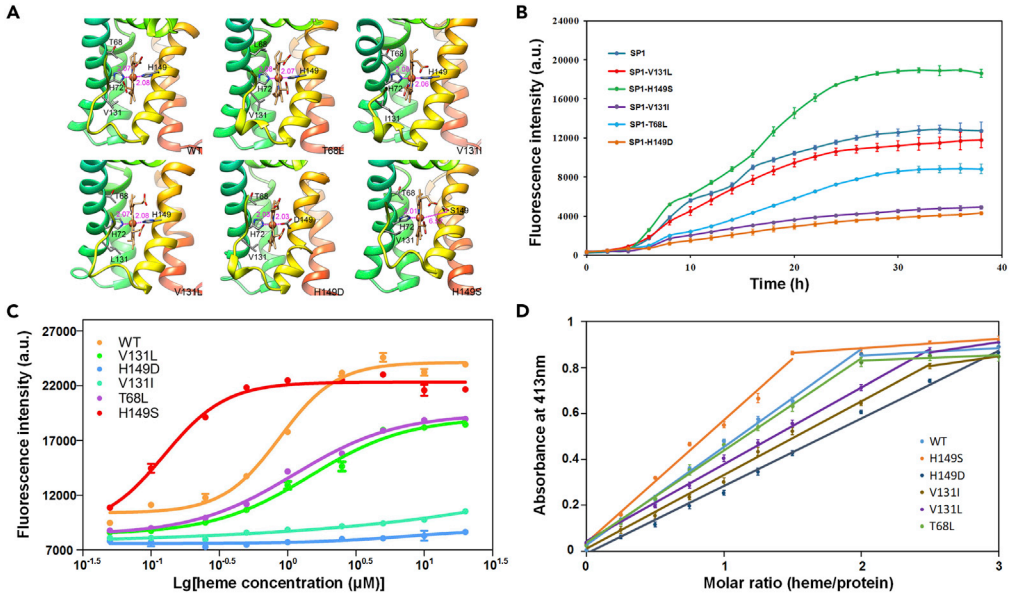

E

	H149S	WT	T68L	V131L	H149D	V131I
Dynamic range	1.49	1.32	1.28	1.29	**	**
Sensitivity	1.921	2.075	0.9489	1.162	**	**
EC_{50} (μM)	0.1245	0.8745	1.237	1.121	**	**

Figure 3. Characterization of Heme Biosensors with Different HrtR Variations

(A) The equilibrated conformations of the heme-binding regions of the wild-type and mutated HrtR (V131I, V131L, T68L, H149D, H149S) derived from molecular dynamics simulations.

(B) Time-dependent GFP expression intensity under the regulation of HrtR mutants H149D, H149S, V131L, V131I, T68L.

(C) Fluorescence of mutants changes after 8 h cultivation with different concentrations of heme.

(D) Changes in absorbance at 413 nm after titration of mutants with heme at different concentrations. Proteins final concentration was 5 μM.

(E) The Dynamic range, Sensitivity, and EC_{50} of mutants. Dynamic range is the ratio of rising fluorescence to background fluorescence, Sensitivity is the slope at EC_{50}. Error bars represent ±1 SD from the mean of three replicate cultures.

Molecular docking and molecular dynamics simulation revealed the binding affinity change of HrtR and its mutants at the molecular level. Molecular dynamics (Mazumder and Case, 2007) simulations demonstrated that replacing the original T68 or V131 with bulkier leucine or isoleucine residues showed marginal effect on the coordinate bonding between heme and HrtR histidines (H72 and H149) (Figure 3A). However, the binding affinity between heme and HrtR became more energetically unfavorable caused by increased steric repulsions (Table S2). The H149D mutation led to an apparent decrease of the coordinate bond lengths (Figure 3A) and consequently a dramatic increase of steric repulsion with most unfavorable binding free energy (Table S2). In contrast, the H149S mutation resulted in a five-coordinate heme-binding complex in which heme formed most energetically favorable binding with the H149S mutant by locating at a much more relaxed hydrophobic pocket (Table S2 and Figure 3A). The binding free energy result showed that the ligand-binding affinity of the mutants followed the order of H149S > WT > V131L > T68L > V131I > H149D. The trend is consistent with the results of our *in vitro* and *in vivo* experiments.

Design and Construction of a Heme-Responsive Regulatory System

The heme-responsive regulatory system was designed by incorporation of heme biosensor with CRISPRi regulation. We synthesized a hybrid promoter containing the DNA-binding site (*hrtO*) of HrtR, whereas HrtR expression was driven by a constitutive promoter (Figure 4). The expression of dCas9 and sgRNA is driven by *hrtO*-hybrid promoters with the cis-regulatory *hrtO*-operator sequence located within or adjacent to the promoter. The general mechanism of the constructed system is depicted in Figure 4. In the early growth period, heme is absent/low, the constitutively expressed HrtR binds to the *hrtO*, which hinders the expression of CRISPRi. When heme is synthesized and accumulated, it interacts with HrtR and allows it dissociate from *hrtO* of *dcas9* promoter, resulting in dCas9 expression that inhibits target genes guiding

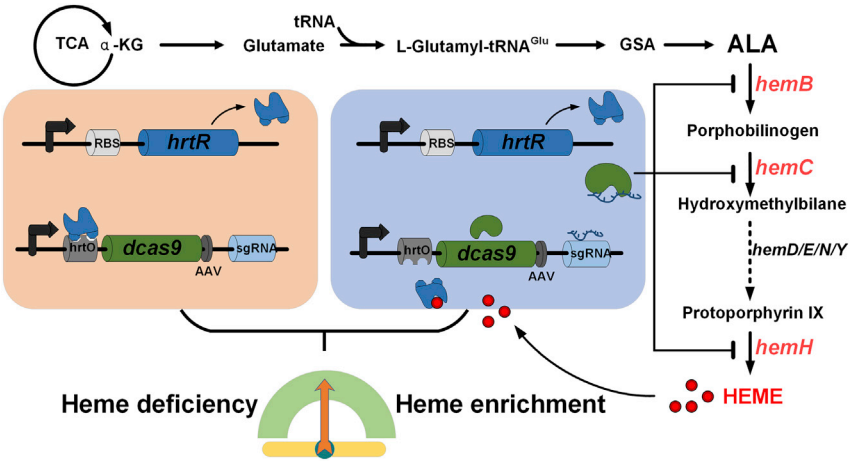

Figure 4. Process of the Heme-Responsive Dynamic Regulation System: HrtR Sensed Excess Heme and Dissociated from *hrtO*, Protein dcas9 Inhibited Target Gene Expression and Reduced the Intracellular Heme Concentration

Low level of heme results in HrtR turning off the expression of CRISPRi by recombining to *hrtO*.

by sgRNA. This further leads to the reduced heme synthesis. Again, low levels of heme results in more HrtR binding to *hrtO* and turns off CRISPRi gradually, which leads to the increased expression of target gene and the constant increase of intracellular heme. The spontaneous cycle of the system ensures the feasibility of dynamic regulation of heme biosynthesis. To increase the system turnover rate, a degradation tag AAV was added to the C terminus of the dcas9 protein.

Red fluorescent protein mKATE2 was used as the second marker protein to characterize the inhibition effect of CRISPRi. Similar to the design above, HrtR controlled the expression of CRISPRi and sgRNA; sgRNA was artificially designed with a complementary region to *mkate2*. Degradation tags LAA were added to the C terminus of mKATE2 to facilitate the turnover. Thus, red fluorescence intensity (i.e., the inhibitory effect of the system) can reflect the intracellular heme concentration change (Figure 5A). Five promoters with different strengths from the iGEM promoter library were selected to initiate expression of *dcas9*, and two different sgRNA targeting different positions of *mkate2* were selected to guide dcas9 (Figure S1). Compared with strains containing sgRNA-A and control strains, the strains containing sgRNA-B located between RBS and promoter of *mkate2* showed lower red fluorescence intensity. Among them, the strain containing the promoter BBa-J23110 showed the lowest fluorescence intensity, which means that it had the best inhibition of mKATE2 (Figure 5B). So, the promoter BBa-J23110 and sgRNA-B were selected for next experiments.

Dynamic Pathway Regulation Using the Heme-Responsive Regulation System

To investigate the dynamic regulation pattern of this system, an sgRNA targeting the *hemB* was designed (Figure S2). When *hemB* is inhibited, the intracellular heme concentration is reduced and CRISPRi expression is turned off, thereby canceling *hemB* inhibition. mKATE2 can be the visualization of the expression of *hemB* via the change of fluorescence. Similarly, in order to find the most suitable inhibition site for *hemB*, three various sgRNAs targeting different positions of *hemB* were used for further screening (Figure 6A). Three constructions were used as blank controls: SH0 (only contained sgRNA targeting *hemB* rather than *mkate2*); SB4 (only contained sgRNA targeting *mkate2* rather than *hemB*); SOH2 (removed off the *hrtO* site within the promoter of CRISPRi system, resulting the constitutive expression of dcas9 and sgRNA) (Figures S1 and S2). The red fluorescence intensity of SH0 was the highest and that of SOH2 was the lowest. The strains in which *hemB* was inhibited had a higher fluorescence intensity than SB4 (Figure 6B). This indicated that the CRISPRi had a significant inhibitory effect on mKATE2 in normal heme accumulating *E. coli*. When *hemB* was inhibited, the intracellular heme concentration decreased, less dcas9 and sgRNA were expressed, resulting in increase in the red fluorescence intensity. This was in line with our design and proved the effectiveness of the synthetic regulatory system.

To visualize the *in vivo* fluctuation of the gene expression, two sgRNAs simultaneously affected by *in vivo* heme concentration were designed to target *mkate2* and *hemB*, respectively. According to our design,

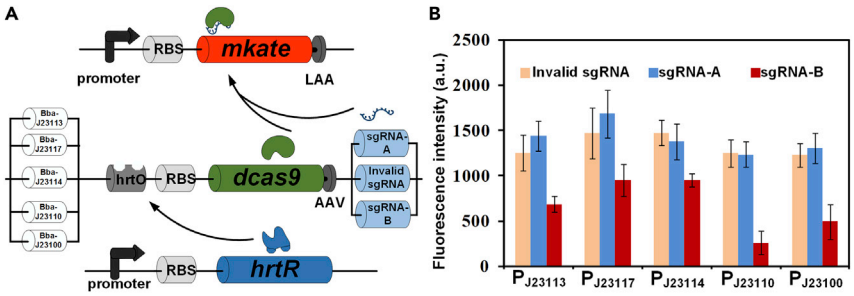

Figure 5. Optimization of CRISPRi Action Site and Expression Intensity in Heme Regulatory System

(A) Schematic representation of the dynamic regulation system represented by the reporter mKATE2.

(B) Red fluorescence in strains containing different promoters of *dcas9* and different sgRNA. Error bars represent ±1 SD from the mean of three replicate cultures.

dynamic regulation of *hemB* made the heme accumulation exhibit an oscillatory changing pattern and so does the expression of *hemB* and *mkate2*. However, results showed that the strain in which *hemB* was inhibited (SH2) had no dynamic fluctuations of red fluorescence. This may be due to the low intracellular heme concentration. To improve intracellular heme concentration, *hemA* from *Salmonella arizona* and *hemL* from *E. coli* were added to SH2 to obtain SH2-AL. No significant fluorescence fluctuations were observed again in SH2-AL. To solve this problem, we changed the promoter and RBS of mKATE2 to reduce the expression of *mkate2*. Finally, obvious fluctuations of fluorescence intensity were observed (Figure 6C). Among them, SH2-AL-2 (promoter: BBa-J23101, RBS: B0032) showed a significant fluorescence intensity change. These results indicated that the synthetic regulatory system can dynamically regulate metabolic pathway by perturbing the genes expression.

To further verify the dynamic regulation in different aspects, real-time fluorescence quantitative PCR was used to analyze the expression of *hemB* and *dcas9* at the transcriptional level. SH2-AL-2 was cultivated in a shake flask with 50 mL of LB medium and sampled for mRNA analysis every 3 h. Fluctuations were observed at different time points in the strains SH2-AL-2 (Figures 6D and 6E). The RT-PCR result proved that the synthetic regulatory system was capable of dynamically regulating dcas9 and *hemB* expression.

Increased ALA Production Using Heme-Responsive Regulatory System

Previous studies in ALA showed that direct overexpression of the key genes in heme synthesis pathway accumulated large quantity of downstream products including heme and porphyrins, which are toxic and affected cell growth (Kang et al., 2011).

Based on SH2-AL, an ALA production strain was constructed by overexpression of *gltW* ($tRNA^{Glu}$, the tRNA responsible for charging glutamic acid), *rhtA* (inner membrane transporter), and *gdhA* (glutamate dehydrogenase) to obtain the strain SH2-ALTG; strains SB4-ALTG (expression of *hemAL*, *gltW*, *gdhA*, *rhtA* on the basis of SB4) and SOH2-ALTG (expression of *hemAL*, *gltW*, *gdhA*, *rhtA* on the basis of SOH2) were set as control. After cultivation, strains SH2-ALTG, SB4-ALTG, SOH2-ALTG have no significant difference in cell growth and glucose consumption. SH2-ALTG accumulated 3.75g/L ALA, which was 1.54-fold of SB4-ALTG (2.42g/L) and 2.09-fold of SOH2-AL (1.8 g/L) (Figure 7A). The results showed that the dynamic regulation of *hemB* contributes to the increased ALA production.

Mutant biosensors with different binding affinity were applied to investigate the effect of ligand-binding affinity on regulation efficiency. As expected, the binding affinity of biosensor had a significant effect on ALA production (Figure 7B). During ALA fermentation, intracellular free heme of these six strains showed a pattern of rise-decrease-rise (Figure 7B). The intracellular heme concentration of the mutant H149D was the highest. At the same time, H149D accumulates the most ALA, 5.35 g/L, which indicates that a high *in vivo* heme level at the early stage of growth is beneficial for cell growth and the ALA production.

Application of Synthetic Regulatory System in Porphyrin and Porphobilinogen Synthesis

Porphyrins play an important role in the fields of medical and materials chemistry (Birnbaum et al., 1995; Karpishin et al., 1994). First, dynamic regulation using heme-responsive biosensor was tried to synthesis PBG by

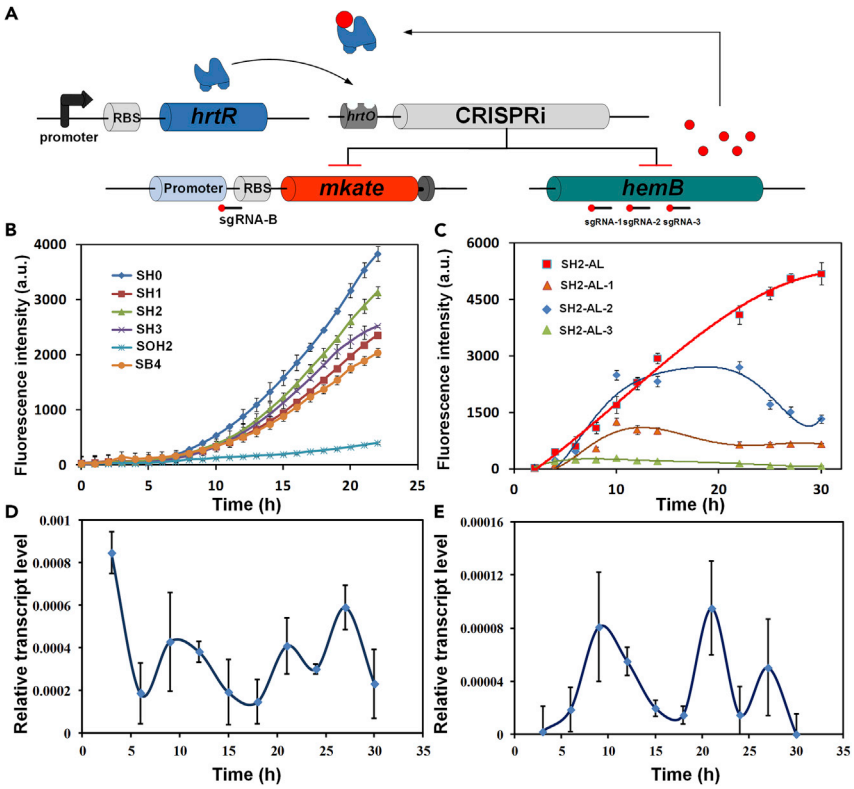

Figure 6. Verification of the Function of the Heme Dynamic Regulation System

(A) Schematic diagram of dynamic control system acting on both *hemB* and *mkate2*.

(B) Red fluorescence intensity of strains containing both sgRNA targeting *mkate2* and *hemB*. SH0 (*mkate2* is not inhibited by CRISPRi), SH1 (sgRNA-A and sgRNA-1), SH2 (sgRNA-A and sgRNA-2), SH3 (sgRNA-A and sgRNA-3), SOH2 (removed *hrtO* based on SH2, making CRISPRi constitutive expression), SB4 (only contains sgRNA-A, no sgRNA targeting *hemB*).

(C) Red fluorescence intensity change after replacing the *mkate2* promoter and RBS, SH2-AL: Ptac and RBS_{B0034}; SH2-AL-1: P_{J23110} and RBS_{B0032}; SH2-AL-2: P_{J23101} and RBS_{B0032}; SH2-AL-3: P_{J23106} and RBS_{B0032}.

(D) The relative expression level of dcas9 in SH2-AL changes with time.

(E) The relative expression level of *hemB* in SH2-AL changes with time. Error bars represent ±1 SD from the mean of three replicate cultures.

designing sgRNA targeting *hemC* (encoding hydroxymethylbilane synthase). PBG accumulation of the strain under the dynamic regulation is 40.25 mg/L, 428.4% higher than that of the un-regulated strain and 80% higher than that of the constitutive-regulated strain (Figure 8B). Meanwhile, the six porphyrin compounds found in the fermentation broth were uroporphyrin (Uro), heptaporphyrin (7-CP), hexaporphyrin (6-CP), pentaporphyrin (5-CP), coproporphyrin I (CopI), and coproporphyrin III (CopIII) (among them, uroporphyrin is a mixture of uroporphyrin I and uroporphyrin III) (Figure 8A). The downstream porphyrin compounds reduced by 55.6% after dynamic regulation of *hemC*, whereas the un-regulated strains accumulated large amounts of porphyrins. Mutants (H149D, H149S, T69L) were used to investigate the regulation role of different biosensors. Among these HrtR and its mutants, wild-type HrtR was the most effective biosensor on the accumulation of PBG. The intracellular free heme of all dynamic strains showed a fluctuation trend with time. The intracellular free heme concentration of H149D was the highest within 30 h (Figures S6B and S6D).

We also designed sgRNA targeting *hemH* (encoding coproporphyrin ferrochelatase). The strain that dynamically regulates *hemH* (SAL-H), strain constitutively inhibiting *hemH* (SAL-HO) and SB4-AL were used for fermentation. The strain with dynamic regulatory system accumulated 65% higher porphyrin compounds than the control strains. The mutants T68L resulted in the highest porphyrin production and reached 3,263.29 μg/L (Figure 8C).

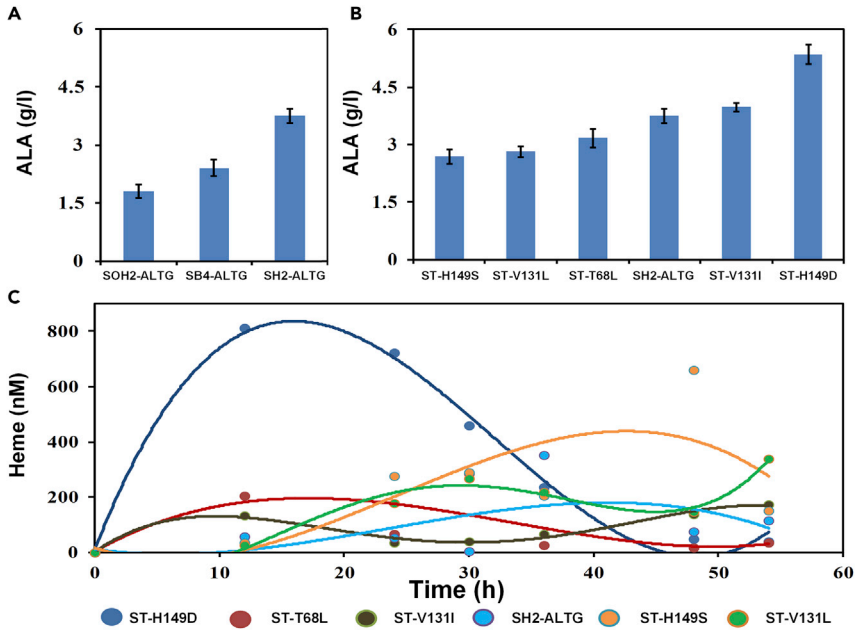

Figure 7. The Application of Heme Dynamic Regulation System in ALA Production

(A) Improvement of ALA production through regulation of *hemB* by heme dynamic regulation system. SOH2-ALTG: Mssing *hrtO*, constitutive expression of CRISPRi, *hemB* was continuously inhibited; SB4-ALTG: without sgRNA targeting *hemB*, *hemB* was not inhibited; SH2-ALTG: *hemB* was regulated by dynamic regulation system.

(B) The ALA production of the engineered strains in which *hemB* was, respectively regulated by wild-type and five HrtR mutants. Strains ST-H149S, ST-V131L, ST-T68L, ST-V131I, and ST-H149D have amino acid mutations that occurred on the basis of SH2-ALTG.

(C) Intracellular free heme concentration curve of fermentation strain. Error bars represent ±1 SD from the mean of three replicate cultures.

DISCUSSION

Biosensors with suitable sensitivity and threshold are the key for regulating the pathway dynamically and precisely. Since heme may act as an allosteric molecule that binds to regulatory proteins and regulate the heme biosynthesis, degradation, and transportation, a universal heme-responsive biosensor can be designed and constructed. Initially, two prokaryotic heme-responsive proteins were selected: iron response regulator (Irr) from *Rhizobium leguminosarum* (Hamza et al., 1998) and HrtR from *Lactococcus lactis*. However, Irr has more than two Heme Regulatory Motifs (Lohrmann et al., 2019) and was also affected by iron level (Singleton et al., 2010), which resulted in complexity and uncertainty. Thus, it was finally discarded after several trials.

To characterize the function of heme-responsive biosensor, a dose-response curve dependent on heme concentration should be determined. However, *E. coli* K-12 strains have no natural heme uptake system. To address this issue, we employed multi-copy integrated *hemA/hemL* strains that can provide different *in vivo* heme concentration (Cui et al., 2019). The positive correlation between the green fluorescence intensity and the *in vivo* heme concentration was observed and guaranteed the characterization of the regulatory system (Figure 1B). And we tried to express the heme transporter HasA/R from *Serratia marcescens* and the transporter HutA from *Bartonella* in *E. coli*, but this did not work (data not shown); finally, this goal was achieved by using ChuA from *E. coli* O157:H7 EDL933. To tune the binding affinity of heme biosensor, three key sites of HrtR that were supposed to be involved in heme binding were selected for saturated mutation based on the protein structure (Sawai et al., 2012). Evaluating biosensor characteristics is necessary before its application. Based on this, a series of heme-responsive biosensors with different sensitivity and threshold were obtained. Our results proved that modifying the metabolite-binding affinity generated a very clear horizontal shift of the dose-response curve with more than 8-fold EC_{50} change and over 2-fold sensitivity change. Detailed biophysical analysis such as heme titration and molecular dynamics simulation can contribute to revealing strategies for biosensor precise control and operational direction. In a sense, some analysis like molecular dynamics simulation can be effective auxiliary methods.

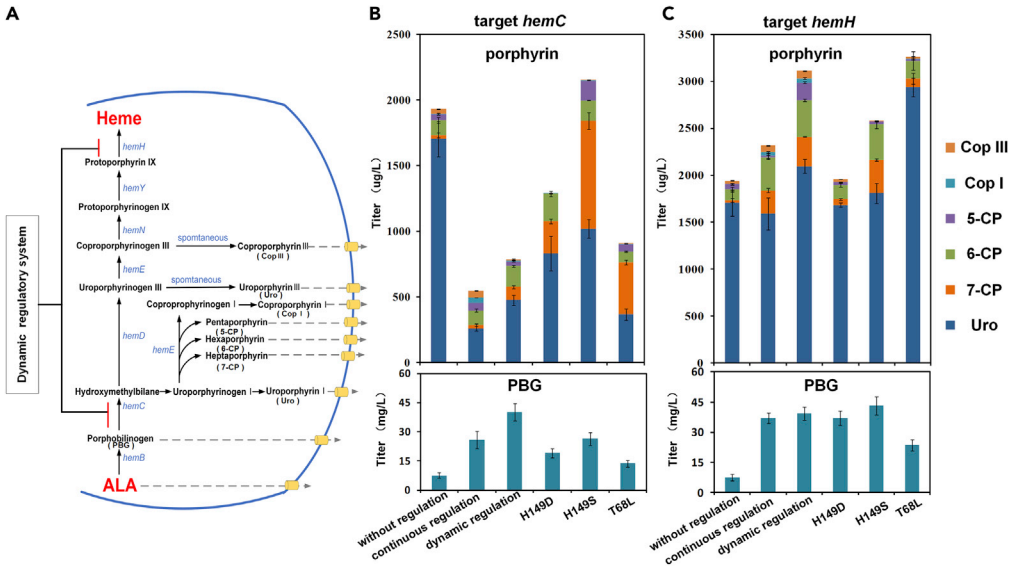

Figure 8. The Application of Heme Dynamic Regulation System in ALA Production

(A) Heme biosynthesis pathway in *Escherichia coli*. *hemA*: glutamyl-tRNA reductase; *hemL*: glutamate-1-semialdehyde aminotransferase; *hemB*: 5-ALA dehydratase; *hemC*: PBG deaminase; *hemD*: uroporphyrinogen III synthase; *hemE*: uroporphyrinogen decarboxylase; *hemN*: coproporphyrinogen III oxidase; *hemY*: protoporphyrinogen oxidase; *hemH*: protoporphyrin ferrochelatase.

(B) PBG and porphyrin productions in dynamic regulation *hemC* strains.

(C) PBG and porphyrin productions in dynamic regulation *hemH* strains. Error bars represent ±1 SD from the mean of three replicate cultures.

The fine-tuned biosensors can be applied in many different pathways. For example, insensitive biosensor needs high heme concentration for dissociation of HrtR from the promoter regulatory site and may be suitable for heme tolerant process. When biosensor H149D was applied in ALA production, 5.35 g/L ALA was obtained. This is the highest ALA production in batch cultivation of *E. coli*.

Compared with antisense RNA (asRNA), RNA interference (RNAi), and protein degradation systems (Cameron and Collins, 2014; Na et al., 2013; Yang et al., 2015), CRISPRi is a robust RNA-guided modulation system that acts at the transcriptional level other than post-transcriptional level and post-translational level. It has many advantages, such as reversibility (Qi et al., 2013). However, it was reported that dCas9 may continuously bind to DNA and thus CRISPRi has a relatively slower turnover rate, which may affect the dynamic regulation efficiency (Qi et al., 2013). Therefore, we designed a degradation tag to the C terminus of *dcas9* to speed up the turnover rate. The oscillatory expression of *hemB* and *dcas9* was observed after this modification (Figures 6D and 6E). The oscillation results under dynamic regulation were also verified by the results of red fluorescence and intracellular heme fluctuation (Figures 6C and 7C).

Since the heme biosynthesis pathway possesses many important compounds, such as B12 (Fang et al., 2018), siroheme, and chlorophyll (Chen et al., 2018), and heme is a small molecule necessary for cell respiration, the heme-responsive regulatory system can be applied for many processes, including basic metabolism (Zhang et al., 2017). In a broader scientific context, biosensor with tailor-made sensitivity provides the possibility of regulating the biological process more dynamically and precisely.

Limitations of the Study

Owing to the transport efficiency of heme transporter and the fact that excessive addition of heme will affect the fluorescence measurement, we could not determine the EC_{50} of the mutants H149D and V131I and only analyzed it by heme titration.

METHODS

All methods can be found in the accompanying Transparent Methods supplemental file.

SUPPLEMENTAL INFORMATION

Supplemental Information can be found online at https://doi.org/10.1016/j.isci.2020.101067.

ACKNOWLEDGMENTS

This work was supported by grants from the National Natural Science Foundation of China (31730003, 31670047, and 31770095), the National Key R&D Program of China (2019YFA0904900), and Young Scholars Program of Shandong University.

AUTHOR CONTRIBUTIONS

J.Z. completed all experiments and the writing of the original manuscript; Z.W. was responsible for the work of molecular dynamics simulation; T.S. participated in the design of the regulatory system and some preliminary work; H.S. and Y.Z. participated in the construction of some plasmids; Q.Q. and Q.W. designed and supervised the entire work and completed the writing of the manuscript.

DECLARATION OF INTERESTS

The authors declare no competing interests.

Received: October 19, 2019
Revised: February 21, 2020
Accepted: April 13, 2020
Published: May 22, 2020

REFERENCES

Baureder, M., and Hederstedt, L. (2013). Heme proteins in lactic acid bacteria. Adv. Microb. Physiol. *62*, 1–43.

Birnbaum, E.R., Grinstaff, M.W., Labinger, J.A., Bercaw, J.E., and Gray, H.B. (1995). On the mechanism of catalytic alkene oxidation by molecular oxygen and halogenated iron porphyrins. J. Mol. Catal. A Chem *104*, L119–L122.

Blazeck, J., and Alper, H.S. (2013). Promoter engineering: recent advances in controlling transcription at the most fundamental level. Biotechnol. J. *8*, 46–58.

Bonyhady, R.E., Hendry, I.A., Hill, C.E., and McLennan, I.S. (1982). Effects of haemin on neurones derived from the neural crest. Dev. Neurosci. *5*, 125–129.

Brophy, J.A., and Voigt, C.A. (2014). Principles of genetic circuit design. Nat. Methods *11*, 508–520.

Cameron, D.E., and Collins, J.J. (2014). Tunable protein degradation in bacteria. Nat. Biotechnol. *32*, 1276–U1149.

Chen, G.E., Canniffe, D.P., Barnett, S.F.H., Hollingshead, S., Brindley, A.A., Vasilev, C., Bryant, D.A., and Hunter, C.N. (2018). Complete enzyme set for chlorophyll biosynthesis in *Escherichia coli*. Sci. Adv. *4*, eaaq1407.

Chen, J.J., and London, I.M. (1981). Hemin enhances the differentiation of mouse 3t3-cells to adipocytes. Cell *26*, 117–122.

Choby, J.E., and Skaar, E.P. (2016). Heme synthesis and acquisition in bacterial pathogens. J. Mol. Biol. *428*, 3408–3428.

Cui, Z.Y., Jiang, Z.N., Zhang, J.H., Zheng, H.H., Jiang, X., Gong, K., Liang, Q.F., Wang, Q., and Qi, Q.S. (2019). Stable and efficient biosynthesis of 5-aminolevulinic acid using plasmid-free *Escherichia coli*. J. Agric. Food Chem. *67*, 1478–1483.

Ding, J.M., Chen, D., Weber, E.T., Faiman, L.E., Rea, M.A., and Gillette, M.U. (1994). Resetting the biological clock: mediation of nocturnal circadian shifts by glutamate and NO. Science *266*, 1713–1717.

Fang, H., Li, D., Kang, J., Jiang, P., Sun, J., and Zhang, D. (2018). Metabolic engineering of *Escherichia coli* for de novo biosynthesis of vitamin B12. Nat. Commun. *9*, 4917.

Feng, Y., Xie, Z., Jiang, X., Li, Z., Shen, Y., Wang, B., and Liu, J. (2018). The applications of promoter-gene-engineered biosensors. Sensors. *18*, 2823.

Fontana, J., Dong, C., Ham, J.Y., Zalatan, J.G., and Carothers, J.M. (2018). Regulated expression of sgRNAs tunes CRISPRi in *E. coli*. Biotechnol. J. *13*, e1800069.

Frunzke, J., Gatgens, C., Brocker, M., and Bott, M. (2011). Control of heme homeostasis in corynebacterium glutamicum by the two-component system HrrSA. J. Bacteriol. *193*, 1212–1221.

Glick, B.R. (1995). Metabolic load and heterologous gene expression. Biotechnol. Adv. *13*, 247–261.

Hamza, I., Chauhan, S., Hassett, R., and O'Brian, M.R. (1998). The bacterial irr protein is required for coordination of heme biosynthesis with iron availability. J. Biol. Chem. *273*, 21669–21674.

Han, Y., Meyer, M.H., Keusgen, M., and Klug, G. (2007). A haem cofactor is required for redox and light signalling by the AppA protein of *Rhodobacter sphaeroides*. Mol. Microbiol. *64*, 1090–1104.

Kang, Z., Wang, Y., Gu, P.F., Wang, Q., and Qi, Q.S. (2011). Engineering *Escherichia coli* for efficient production of 5-aminolevulinic acid from glucose. Metab. Eng. *13*, 492–498.

Karpishin, T.B., Grinstaff, M.W., Komarpanicucci, S., Mclendon, G., and Gray, H.B. (1994). Electron-transfer in cytochrome-C depends upon the structure of the intervening medium. Structure *2*, 415–422.

Layer, G., Reichelt, J., Jahn, D., and Heinz, D.W. (2010). Structure and function of enzymes in heme biosynthesis. Protein Sci. *19*, 1137–1161.

Lechardeur, D., Cesselin, B., Liebl, U., Vos, M.H., Fernandez, A., Brun, C., Gruss, A., and Gaudu, P. (2012). Discovery of intracellular heme-binding protein HrtR, which controls heme efflux by the conserved HrtB-HrtA transporter in *Lactococcus lactis*. J. Biol. Chem. *287*, 4752–4758.

Liu, D., Evans, T., and Zhang, F. (2015a). Applications and advances of metabolite

biosensors for metabolic engineering. Metab. Eng. *31*, 35–43.

Liu, D., Xiao, Y., Evans, B.S., and Zhang, F. (2015b). Negative feedback regulation of fatty acid production based on a malonyl-CoA sensor-actuator. ACS Synth. Biol. *4*, 132–140.

Lohrmann, V., Ohl, M., Michalik, P., Pitts, J.P., Jeanneau, L., and Perrichot, V. (2019). Notes on rhopalosomatid wasps of Dominican and Mexican amber (Hymenoptera: Rhopalosomatidae) with a description of the first fossil species of Rhopalosoma Cresson, 1865. Foss Rec. *22*, 31–44.

Mahr, R., and Frunzke, J. (2016). Transcription factor-based biosensors in biotechnology: current state and future prospects. Appl. Microbiol. Biotechnol. *100*, 79–90.

Mannan, A.A., Liu, D., Zhang, F., and Oyarzun, D.A. (2017). Fundamental design principles for transcription-factor-based metabolite biosensors. ACS Synth. Biol. *6*, 1851–1859.

Martin, V.J., Pitera, D.J., Withers, S.T., Newman, J.D., and Keasling, J.D. (2003). Engineering a mevalonate pathway in *Escherichia coli* for production of terpenoids. Nat. Biotechnol. *21*, 796–802.

Mazumder, D., and Case, D.A. (2007). AMBER Score in DOCK6: application of molecular dynamics simulations and implicit solvent model (GB/SA) in protein-ligand docking. Abstr. Pap. Am. Chem. S *233*, 20.

Na, D., Yoo, S.M., Chung, H., Park, H., Park, J.H., and Lee, S.Y. (2013). Metabolic engineering of *Escherichia coli* using synthetic small regulatory RNAs. Nat. Biotechnol. *31*, 170–174.

Qi, L.S., Larson, M.H., Gilbert, L.A., Doudna, J.A., Weissman, J.S., Arkin, A.P., and Lim, W.A. (2013). Repurposing CRISPR as an RNA-guided platform for sequence-specific control of gene expression. Cell *152*, 1173–1183.

Qi, Z., Hamza, I., and O'Brian, M.R. (1999). Heme is an effector molecule for iron-dependent degradation of the bacterial iron response regulator (Irr) protein. Proc. Natl. Acad. Sci. U S A *96*, 13056–13061.

Ryter, S.W., and Tyrrell, R.M. (2000). The Heme synthesis and degradation pathways: role in oxidant sensitivity - heme oxygenase has both pro- and antioxidant properties. Free Radic. Bio. Med. *28*, 289–309.

Sawai, H., Yamanaka, M., Sugimoto, H., Shiro, Y., and Aono, S. (2012). Structural basis for the transcriptional regulation of heme homeostasis in *Lactococcus lactis*. J. Biol. Chem. *287*, 30755–30768.

Shelver, D., Kerby, R.L., He, Y.P., and Roberts, G.P. (1997). CooA, a CO-sensing transcription factor from *Rhodospirillum rubrum*, is a CO-binding heme protein. Proc. Natl. Acad. Sci. U S A *94*, 11216–11220.

Shen-Orr, S.S., Milo, R., Mangan, S., and Alon, U. (2002). Network motifs in the transcriptional regulation network of *Escherichia coli*. Nat. Genet. *31*, 64–68.

Singleton, C., White, G.F., Todd, J.D., Marritt, S.J., Cheesman, M.R., Johnston, A.W., and Le Brun, N.E. (2010). Heme-responsive DNA binding by the global iron regulator Irr from *Rhizobium leguminosarum*. J. Biol. Chem. *285*, 16023–16031.

Taylor, N.D., Garruss, A.S., Moretti, R., Chan, S., Arbing, M.A., Cascio, D., Rogers, J.K., Isaacs, F.J., Kosuri, S., Baker, D., et al. (2016). Engineering an allosteric transcription factor to respond to new ligands. Nat. Methods *13*, 177–183.

Trabelsi, H., Koch, M., and Faulon, J.L. (2018). Building a minimal and generalizable model of transcription factor-based biosensors: showcasing flavonoids. Biotechnol. Bioeng. *115*, 2292–2304.

Tsiftsoglou, A.S., Tsamadou, A.I., and Papadopoulou, L.C. (2006). Heme as key regulator of major mammalian cellular functions: molecular, cellular, and pharmacological aspects. Pharmacol. Therapeut. *111*, 327–345.

Tyo, K.E., Ajikumar, P.K., and Stephanopoulos, G. (2009). Stabilized gene duplication enables long-term selection-free heterologous pathway expression. Nat. Biotechnol. *27*, 760–765.

Xu, P., Li, L., Zhang, F., Stephanopoulos, G., and Koffas, M. (2014). Improving fatty acids production by engineering dynamic pathway regulation and metabolic control. Proc. Natl. Acad. Sci. U S A *111*, 11299–11304.

Yang, Y.P., Lin, Y.H., Li, L.Y., Linhardt, R.J., and Yan, Y.J. (2015). Regulating malonyl-CoA metabolism via synthetic antisense RNAs for enhanced biosynthesis of natural products. Metab. Eng. *29*, 217–226.

Zhang, F., Carothers, J.M., and Keasling, J.D. (2012). Design of a dynamic sensor-regulator system for production of chemicals and fuels derived from fatty acids. Nat. Biotechnol. *30*, 354–359.

Zhang, T.T., Bu, P.L., Zeng, J., and Vancura, A. (2017). Increased heme synthesis in yeast induces a metabolic switch from fermentation to respiration even under conditions of glucose repression. J. Biol. Chem. *292*, 16942–16954.

iScience, Volume *23*

Supplemental Information

Tuning the Binding Affinity of Heme-Responsive Biosensor for Precise and Dynamic Pathway Regulation

Jian Zhang, Zhiguo Wang, Tianyuan Su, Huanhuan Sun, Yuan Zhu, Qingsheng Qi, and Qian Wang

Supplementary Files

Tuning the binding affinity of heme-responsive biosensor for precise and dynamic pathway regulation

Jian Zhang[1], Zhiguo Wang[2], Tianyuan Su[1], Huanhuan Sun[1], Yuan Zhu[1], Qingsheng Qi[1,3*], Qian Wang[1*]

1. State Key Laboratory of Microbial Technology, National Glycoengineering Research Center, Shandong University, Qingdao 266237, P. R. China
2. Institute of Ageing Research, School of Medicine, Hangzhou Normal University, Hangzhou, 311121, P. R. China
3. CAS Key Lab of Biobased Materials, Qingdao Institute of Bioenergy and Bioprocess Technology, Chinese Academy of Sciences, Qingdao 266101, P. R. China

*Corresponding authors:

Qingsheng Qi

Tel: 0532-58632580, E-mail: qiqingsheng@sdu.edu.cn;

Qian Wang

Tel: 0532-58631580, E-mail: qiqi20011983@gmail.com, lead contact author

TRANSPARENT METHOD

General procedure

All the strains used in this study were summarized in Supplementary Table S3. Molecular cloning and manipulation of plasmids were done with *E. coli* DH5α. All the plasmids and oligonucleotides used in this work were listed in Supplementary Table S4 and Table S5.

Construction of heme biosensor

To construct a related plasmid that characterizes HrtR function, the *hrtR* and *gfp* genes were generated by PCR with primers hrtR-F/hrtR-R, gfp-F/gfp-R, respectively. Chloramphenicol resistance gene and p15A ori were cloned with primers p15A-F/p15A-R using plasmid pACYC184 as the template. Then the three fragments were assembled together using the Gibson method(Gibson et al., 2009) to obtain the plasmid P1. To construct plasmids P0, P2, P3 and P4, the resulting fragments were transformed into *E. coli* DH5α after the treatment by T4 PNK and T4 ligase, which generated by primers p0-F/p0-R, p2-F/p2-R, p3-F/p3-R, p4-F/p3-R were performed, respectively.

Construction and characterization of HrtR saturation mutant library

All HrtR mutants were obtained by using plasmid P1 as template, the primers used for the mutation are listed in Supplementary Table S5. Phanta Max Super-Fidelity DNA Polymerase P505 (Vazyme Biotech Co.,Ltd) was used in all PCR reactions. Resulting fragment was assembled using the Gibson method. The obtained plasmids were transferred into DH5α, respectively, and the obtained strain was cultured in a 24-well plate. After 24 hours of culture, the green fluorescence intensity was detected by a microplate reader. (GFP: exciting light: 485nm, emission light: 528nm).

Construction and optimization of the regulatory system

The strain that regulation *mkate2* contains plasmids PDMGn (n=1, 2, 3, 4, 5) and PSX (X=A,B,O). For pDMG1 construction, chloramphenicol resistance gene and p15A ori were amplified with primers ori-F/ori-R-1. Promoter BBa-J23113 of dcas9 was included in the primer ori-R-1. *dcas9* and *mkate2* gene were cloned with primers dcas9-F/dcas9-R and

mkate-F/mkate-R, degradation tags AAV (AANDENYAAAV) and LAA (AANDENYALAA) are added to the corresponding primers, respectively. Fragments containing different promoters were fused by overlap PCR with primer mkate-F2 and ori-R-1. Resulting fragment was assembled using the Gibson method. Similarly, promoters BBa-J23117, Ba-J23114, Ba-J23110 and Ba-J23100 were contained in primers ori-R-2, ori-R-3, ori-R-4 and ori-R-5, respectively. The construction method of pDMG2, pDMG3, pDMG4 and pDMG5 were the same as above. The construction method of pDMG0 is the same as that of P0, using pDMG4 as a template and primers pair pdmg0-F/pdmg0-R. PDMG4 was cloned as a template using primers M1-F and M1-R, M2-F and M2-R, M2-F and M3-R, resulting fragment were transformed into *E. coli* DH5α after the treatment by T4 PNK and T4 ligase to obtain the plasmid pDMG4-1, pDMG4-2 and pDMG4-3.

For pSA and pSB construction, sgRNA-A and sgRNA-B were cloned with primer pairs sgrna-a-F/sgrna-R, sgrna-b-F/sgrna-R, respectively. *hrtR* was amplified using primer sensor-F and sensor-R. then *hrtR* and Different sgRNAs were assembled using the Gibson method with the plasmid puc19 digested with *Bam*HI. The construction method of pSO is the same as that of P0, using pSIB as a template and psio-F/psio-R as primers.

Plasmids PBHn (n=1, 2, 3) was constructed by adding sgRNA targeting *hemB* to PSB. Different sgRNAs targeting *hemB* were amplified using primers sg-1-F/sg-1-R, sg-2-F/sg-2-R, sg-3-F/sg-3-R, respectively. pSB cloned with primers site-F/site-R was used as the backbone. SgRNA-1, sgRNA-2 and sgRNA-3 were assembled using the Gibson method with the backbone, respectively. At the same time, we replaced the backbone with pSO based on pBH2 to obtain the plasmid pOH2. Remove the *hrtO* from the primer sg-2-F and use it to amplify with sg-1-R, resulting fragment was assembled using the Gibson method with the backbone pSB to obtain the plasmid pOBH2.

The obtained plasmids were transferred into DH5α, respectively, the specific conditions of the plasmid contained in the strain refer to Supplementary Table S3, And the obtained strain was cultured in a 24-well plate and the red fluorescence intensity was detected in real time using a microplate reader (mKATE: exciting light: 590nm, emission light: 645nm).

Construction of ALA, PBG and Porphyrin biosynthesis system

The gene *hemA* from *Salmonella Arizona* and *hemL* from *E. coli* was cloned with primers AL-F/AL-R using pDAL as a template. The plasmid pSB, pSBH2 and pOSBH2 were amplified using primers 10B-gj-F/10B-gj-R, respectively. After digestion with *Xho*I and *Not*I, *hemA-hemL* were cloned into the above linearized plasmids cut with *Xho*I and *Not*I to obtain the plasmid pSBAL, pBH2AL and pOBH2AL. For pBH2ALT construction, *gltW* was cloned with primers tRNA-F/tRNA-R, the backbone was amplified with primers tRNA-gj-F/tRNA-gj-R using pBH2AL as a template. The two fragments were assembled using the Gibson method. The *gdhA* gene in *E. coli* was cloned and integrated into the PCLA plasmid by Gibson method to construct the PCLAG plasmid.

The pCAL and PHAL were cloned with primers CAL-F/CAL-R and HAL-F/HAL-R using pSBAL and as a template, resulting fragment were transformed into *E. coli* DH5α after the treatment by T4 PNK and T4 ligase. pOCAL and POHAL were obtained using the same method, using pCAL and pHAL as a template and CO-F/CO-R and HO-F/ HO-R as primers. The obtained plasmids were transferred into DH5α, respectively, the specific conditions of the plasmid contained in the strain refer to Supplementary Table S3. The medium composition and culture conditions used in the fermentation process were the same as the previous report. ALA and PBG concentration were analyzed using modified Ehrlich's reagent(Kang et al., 2011). Porphyrin compounds were detected by HPLC.

Quantitative real-time PCR (RT-PCR)

The primers studied in this work were listed in Supplementary Table S5. The message RNA (mRNA) level was measured by RT-PCR. The Sample for extracting mRNA were harvested and frozen immediately at -80 ℃. mRNA of hemB and dcas9 was extracted using the RNeasy Mini Kit (Tiangen). The cDNA was obtained from reverse transcription and RT-PCR was carried out in a 96-well plate with a total reaction volume of 20 μL per well in QuantStudioTM3 (Thermo Fisher) using an SYBR® Premix Ex Taq™ II (Perfect Real Time), according to manufacturer's specifications (TaKaRa).

Analysis of heme

The cells were cultured in LB medium, and 1 ml was sampled every 6 hours. The obtained sample was disrupted by Automatic sample grinder (Jingxin, Shanghai), and the supernatant was taken after centrifugation. Intracellular heme concentration was determined using Heme Colorimetric Assay Kit (BioVision, USA).

Dose response curve

Mutants were cultured in LB medium supplemented with 0.05μM, 0.1μM, 0.25μM, 0.5μM, 1μM, 2.5μM, 5μM, 10μM and 20μM heme respectively. Cells were cultured in a 96-well plate and the fluorescence intensity was measured at 8h. GraphPad was used to draw the dose response curve and calculate various parameters.

Heme titration

Purification of HrtR and heme titration experiments referred to the methods of Sawai et al (Sawai et al., 2012).

Molecular dynamics

The molecular dynamics(Mazumder and Case) simulations were performed on the heme bound HrtR/mutant dimers (PDB ID: 3VP5)(Sawai et al., 2012) by using the AMBER 12 software(Case et al., 2005). The FF14SB force field(Maier et al., 2015) was applied for the HrtR proteins. The point charges of heme were calculated with antechamber[4] based on the restricted electrostatic potential (RESP) procedure(Bayly et al., 1993). Bonded terms at the Fe center were calculated according to Seminario's method based on second - derivatives(Seminario, 1996; Villarino et al., 2018), the GAFF force field(Wang et al., 2004) was adopted for the remaining atoms of heme. The binding complexes were individually immersed into the center of a truncated octahedron box of TIP3P water molecules with a margin distance of 10.0 Å, Na^+ counterions were added with the AMBER XLEAP module to keep system in electric neutrality(Case et al., 2005). Each system was firstly energy minimized using the steepest descent method for 5000 steps with the binding complex restricted by a harmonic constraint of 100 kcal·$mol^{-1}Å^{-2}$. A further conjugate gradient minimization of 5000 steps was performed with no constraint. Then the system was gradually heated from 0 K to 300 K under the NVT ensemble over a period of 1 ns, during

which the Langevin thermostat with a coupling coefficient of 1.0 ps and a weak constraint of 10 kcal·mol^{-1}Å^{-2} on the binding complex was applied. Each model was subjected to an equilibrium simulation for 1 ns with no constraint and then a 20 ns production MD simulation under NPT ensemble. Periodic boundary conditions were applied. System temperature was kept 300 K using the Berendsen thermostat with a time constant of 1 ps. Isotropic constant pressure was maintained using Berendsen pressure coupling algorithm with a time constant of 1 ps. Hydrogens involved in covalent bonds were constrained by the SHAKE algorithm(Ryckaert J P 1976). The long-range electrostatic interactions were treated by the Particle Mesh Ewald (PME) method(Essmann et al., 1995). The cutoffs for long-range electrostatic and Van der Waals interactions were both set to 10.0 Å. The time step was set to 2 fs, the coordinates were saved every 1 ps to record the MD trajectory.

Binding free energy

By neglecting the coordinate bonding interactions between HrtR and heme, their intermolecular binding free energy (ΔG_{bind}) was calculated using the molecular mechanics combined with generalized Born and surface area solvation (MM/GBSA) approach(Kollman et al., 2000):

$$\Delta G_{bind} = G_{complex} - (G_{G4} + G_{APC}) \quad (1)$$

$$\Delta G_{bind} = \Delta H - T\Delta S \approx \Delta E_{MM} + \Delta G_{solv} - T\Delta S \quad (2)$$

$$\Delta E_{MM} = \Delta E_{int} + \Delta E_{vdW} + \Delta E_{ele} \quad (3)$$

$$\Delta G_{solv} = \Delta G_{GB} + \Delta G_{SA} \quad (4)$$

Where E_{MM} is the gas phase interaction energy comprising internal strain energy (E_{int}), van der Waals energy (E_{vdW}) and electrostatic energy (E_{ele}). G_{solv} is the solvation free energy comprising contributions form a polar part (G_{GB}) and a nonpolar part (Taverna et al.). ΔE_{int} can be neglected in the current system. ΔG_{GB} was estimated using the generalized Born model with the interior and exterior dielectric constants set to 4 and 80, respectively. ΔG_{SA} was estimated using the LCPO algorithm(Weiser et al., 1999): $\Delta G_{SA} = \gamma\Delta SASA + \beta$, where γ and β were set to 0.0072 and 0, respectively. By performing the normal mode analysis (NMA), $T\Delta S$ that represents the entropy contribution was estimated using the NMODE module. Snapshots were extracted from the last 5 ns trajectories with an interval of 25 ps for the calculations of ΔE_{vdW}, ΔE_{ele}, ΔG_{GB} and ΔG_{SA}. While for the calculation of entropy, only 50 snapshots was evenly extracted from the last 5 ns trajectories due to the expensive computational cost of NMA(Liu et al., 2018).

Supplementary Figures

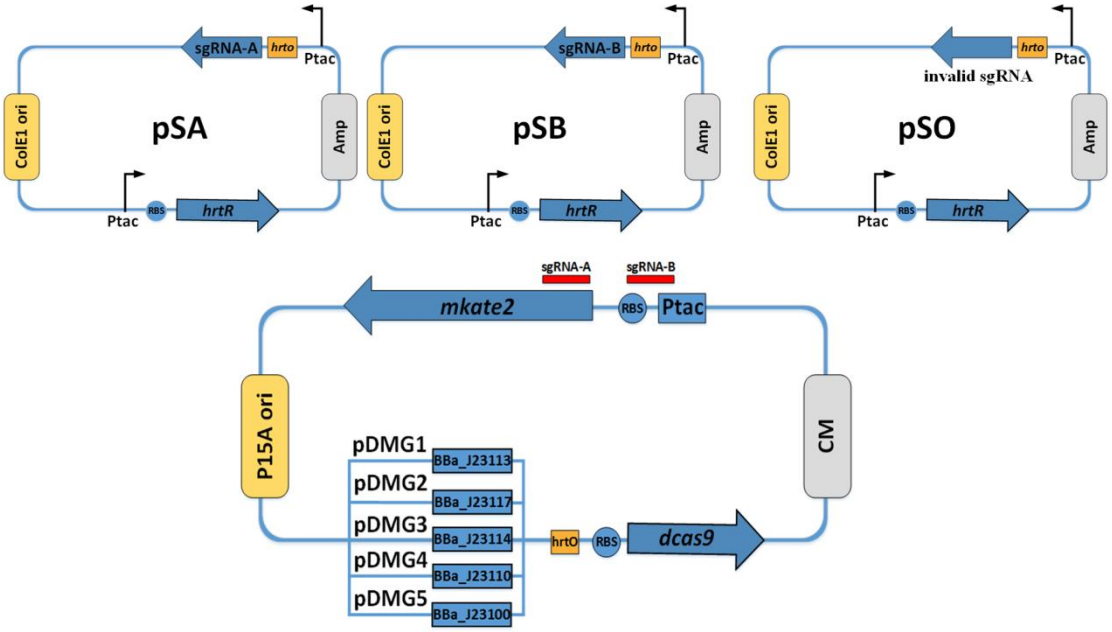

Figure S1: sgRNA-A acts at the 5' end 24bp-44bp of *mkate2*; sgRNA-B acts at the middle of promoter and RBS of *mkate2*; sgRNA-C does not contain a spacer site. Related to Figure 5

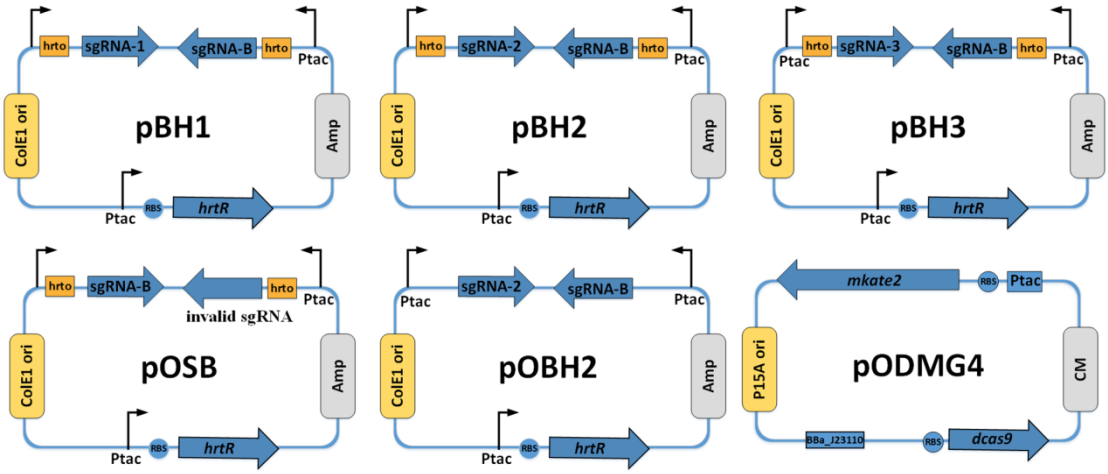

Figure S2: The schematic diagram of plasmids pBHn (n=1,2,3), pOSB, pOBH2, pODMG4. Related to Figure 6

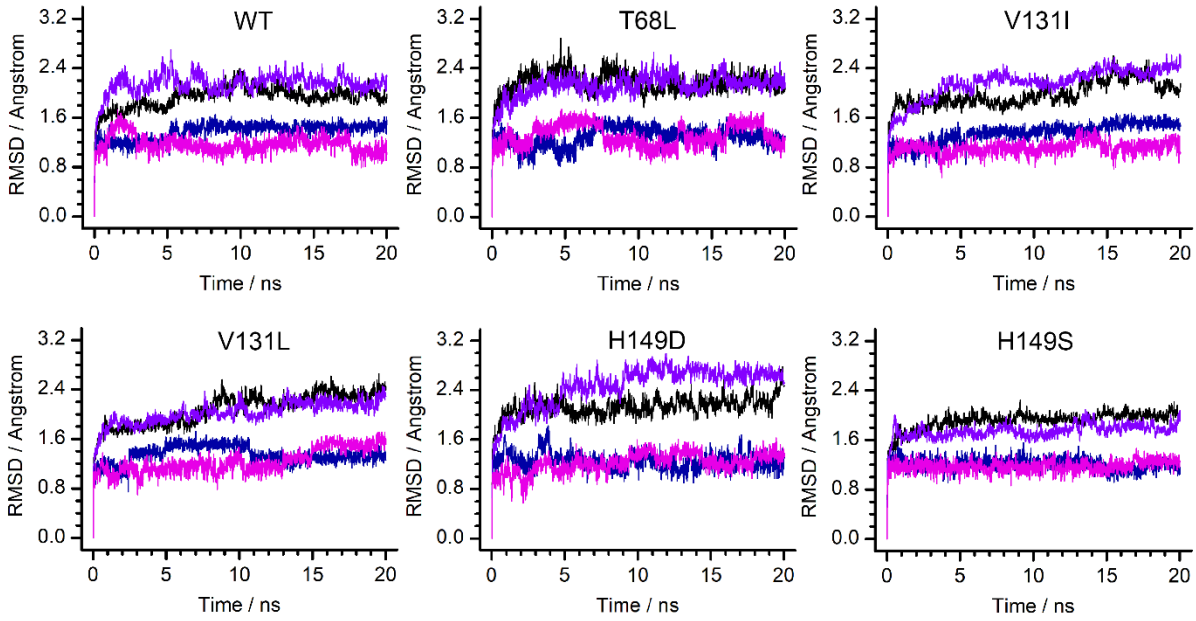

Figure S3,. The root-mean-square deviations (RMSDs) of the HrtR dimer during molecular dynamics. The RMSDs are colored in black and purple for the HrtR proteins in chain A and chain B, respectively. The RMSDs of the heme molecules that bind to the chain A and chain B are colored in navy blue and magenta, respectively. Related to Figure 3

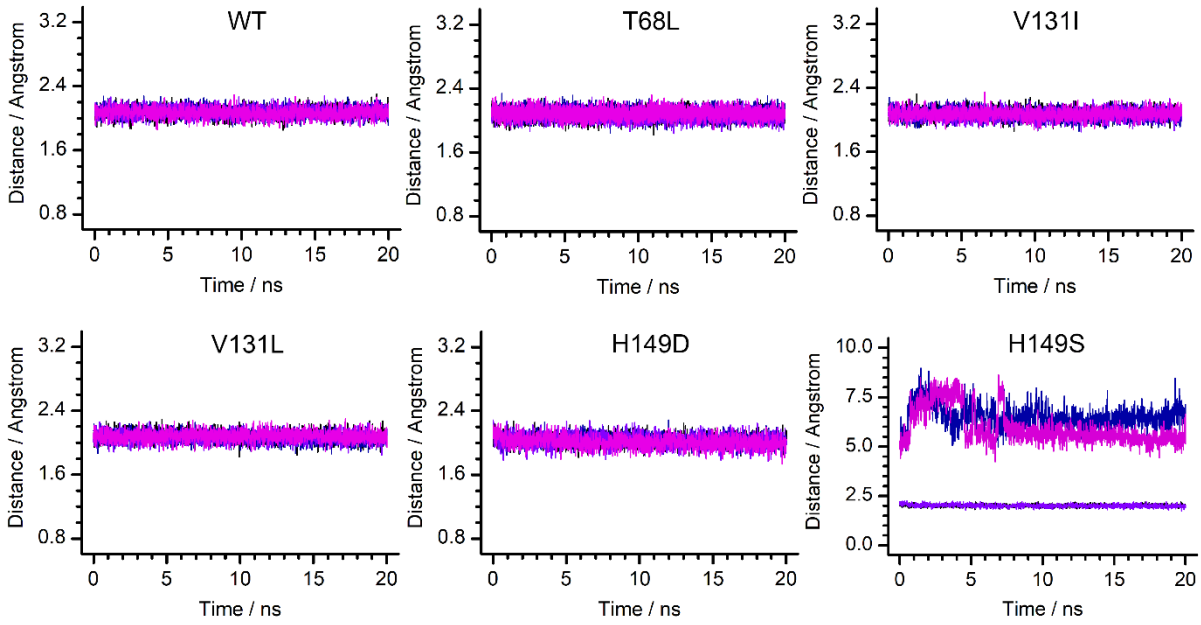

Figure S4. The distances between the heme Fe atom and the HrtR residues. The distance curves between heme Fe atom and NE2 atoms of H72 from chain A and chain B are colored in black and purple, respectively. The distance curves between heme Fe atom and NE2/OD1/OG atoms of H149/D149/S149 from chain A and chain B are colored in navy blue and magenta, respectively. Related to Figure 3

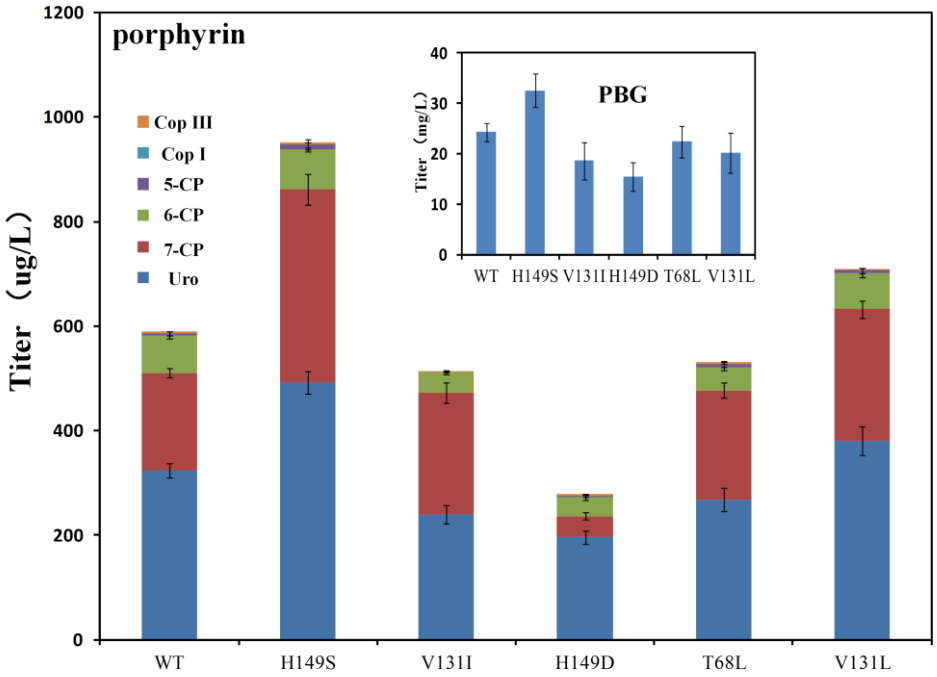

231

232 Figure S5. Accumulation of porphyrins and PBG in different mutant during ALA production;

233 Error bars represent ±1 SD from the mean of three replicate cultures. Related to Figure 7

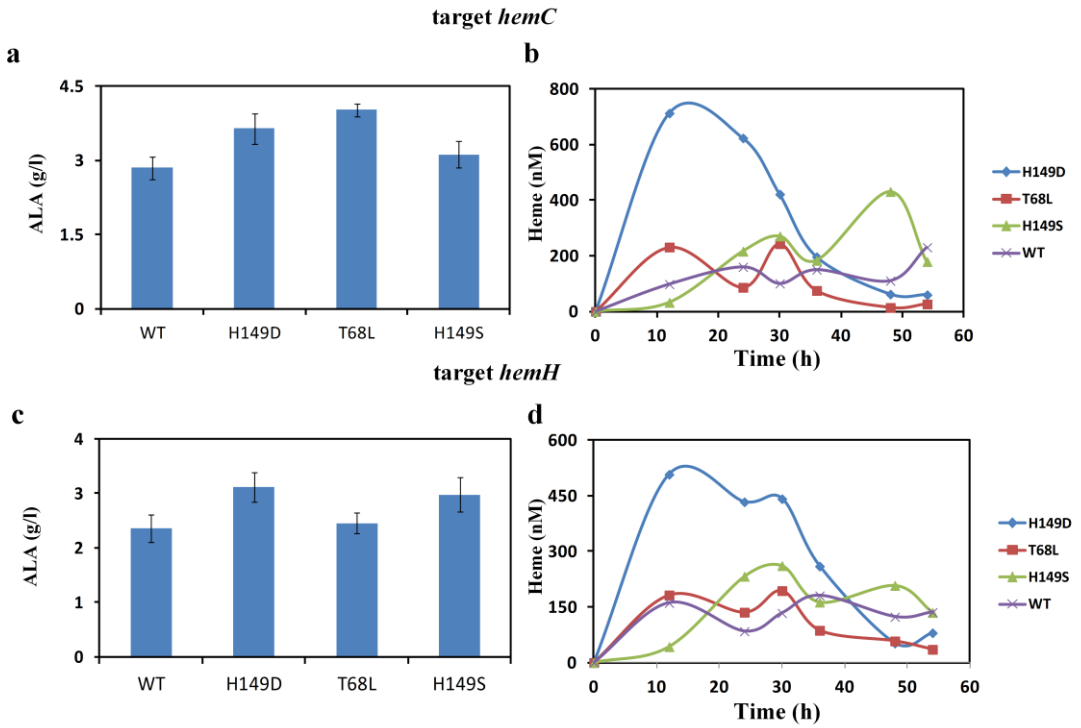

Figure S6. a: Accumulation of ALA in different mutants during PBG production; b: Intracellular free heme concentration curve of the strain target *hemC*; c: Accumulation of ALA in different mutants during porphyrins production; b: Intracellular free heme concentration curve of the strain target *hemH*. Error bars represent ±1 SD from the mean of three replicate cultures. Related to Figure 8

Supplementary Tables

Table S1. Fluorescence intensity of GFP under the control of different mutants. Related to Figure 2

	N	K	T	S	R	I	M	H	Q	P
Thr68	27719	32044	13628	27379	27528	12095	22640	30604	24327	38225
Val131	4518	5690	6159	7516	7545	5576	6671	7692	7153	7427
His149	5081	5930	6374	30161	6607	6347	7628	13628	5281	30290
	L	**D**	**E**	**A**	**G**	**V**	**Y**	**C**	**W**	**F**
Thr68	6937	36889	35757	25694	22389	19316	27781	12065	35333	10994
Val131	14183	5788	5395	9991	5741	13628	9273	6463	10936	11663
His149	6209	4442	4413	6345	6021	7540	7130	7028	7685	6582

Table S2. Binding free energies between HrtR and heme[a]. Related to Figure 3

P450	Energy components[b]						
	ΔE_{ele}	ΔE_{vdW}	ΔG_{GB}	ΔG_{SA}	ΔH	$-T\Delta S$	ΔG_{bind}
WT	190.59	1.69	-155.66	-9.12	27.49	30.09	57.58
T68L	177.64	14.27	-147.91	-8.81	35.19	30.66	65.85
V131I	223.01	6.14	-188.54	-8.89	31.72	34.88	66.60
V131L	138.60	12.36	-111.28	-9.08	30.60	29.25	59.85
H149D	297.42	18.55	-262.79	-8.79	44.39	35.10	79.49
H149S	135.06	-49.53	-118.95	-9.37	-42.78	32.90	-9.88

[a] The binding free energies were calculated by neglecting the coordinate bonding interactions between HrtR and heme since the molecular dynamics method is unproper to compute the intermolecular binding affinity with covalent bond involved. Therefore, the values of ΔG_{bind} presented here represent the binding susceptibility of heme to the HrtR variants instead of absolute binding free energies.

[b] Energies are in kcal·mol^{-1}.

Table S3. Bacterial strains used in this study. Related to Figure 1,2,3,5,6,7 and 8.

Strains	Relevant properties	Source
DH5α		**lab stock**
S1	**MG1655 integrates a copies of *hemA*/*hemL* on the genome**	**lab stock**
S20	**MG1655 integrates 20 copies of *hemA*/*hemL* on the genome**	**lab stock**
S35	**MG1655 integrates 35 copies of *hemA*/*hemL* on the genome**	**lab stock**
S65	**MG1655 integrates 65 copies of *hemA*/*hemL* on the genome**	**lab stock**
S100	**MG1655 integrates 100 copies of *hemA*/*hemL* on the genome**	**lab stock**
S1P1	**S1 harboring P1**	**this study**
S20P1	**S20 harboring P1**	**this study**
S35P1	**S35 harboring P1**	**this study**
S65P1	**S65 harboring P1**	**this study**
S100P1	**S100 harboring P1**	**this study**
SP0	**DH5α harboring P0**	**this study**
SP1	**DH5α harboring P2**	**this study**
SP2	**DH5α harboring P3**	**this study**
SP3	**DH5α harboring P4**	**this study**
SP4	**DH5α harboring P5**	**this study**
SP1-T68L	**DH5α harboring P1-T68L**	**this study**
SP1-V131L	**DH5α harboring P1-V131L**	**this study**
SP1-V131I	**DH5α harboring P1-V131I**	**this study**
SP1-H149D	**DH5α harboring P1-H149D**	**this study**
SP1-H149S	**DH5α harboring P1-H149S**	**this study**
SO1	**DH5α harboring PSO+PDMG1**	**this study**
SO2	**DH5α harboring PSO+PDMG2**	**this study**
SO3	**DH5α harboring PSO+PDMG3**	**this study**
SO4	**DH5α harboring PSO+PDMG4**	**this study**
SO5	**DH5α harboring PSO+PDMG5**	**this study**
SA1	**DH5α harboring PSA+PDMG1**	**this study**
SA2	**DH5α harboring PSA+PDMG2**	**this study**
SA3	**DH5α harboring PSA+PDMG3**	**this study**
SA4	**DH5α harboring PSA+PDMG4**	**this study**
SA5	**DH5α harboring PSA+PDMG5**	**this study**
SB1	**DH5α harboring PSB+PDMG1**	**this study**
SB2	**DH5α harboring PSB+PDMG2**	**this study**
SB3	**DH5α harboring PSB+PDMG3**	**this study**
SB4	**DH5α harboring PSB+PDMG4**	**this study**
SB5	**DH5α harboring PSB+PDMG5**	**this study**
SH0	**DH5α harboring PDMG4+POSB**	**this study**
SH1	**DH5α harboring PDMG4+PBH1**	**this study**
SH2	**DH5α harboring PDMG4+PBH2**	**this study**
SH3	**DH5α harboring PDMG4+PBH3**	**this study**
SOH	**DH5α harboring PODMG4+POBH2**	**this study**
SH2-AL-1	**DH5α harboring PBH2-AL+PDMG4-1**	**this study**
SH2-AL-2	**DH5α harboring PBH2-AL+PDMG4-2**	**this study**
SH2-AL-3	**DH5α harboring PBH2-AL+PDMG4-3**	**this study**
SOH-AL	**DH5α harboring PODMG4+POBH2-AL**	**this study**
SB4-AL	**DH5α harboring PSB-AL+PDMG4**	**this study**

SH2-AL	**DH5α harboring PDMG4+PBH2-AL**	**this study**
SH2-ALT	**DH5α harboring PDMG4+PBH2ALT**	**this study**
SH2-ALTG	**DH5α harboring PDMG4+PBH2ALTG**	**this study**
ST-T68L	**DH5α harboring PDMG4+PBH2ALTG-T68L**	**this study**
ST-V131L	**DH5α harboring PDMG4+PBH2ALTG-V131L**	**this study**
ST-V131I	**DH5α harboring PDMG4+PBH2ALTG-V131I**	**this study**
ST-H149D	**DH5α harboring PDMG4+PBH2ALTG-H149D**	**this study**
ST-H149S	**DH5α harboring PDMG4+PBH2ALTG-H149S**	**this study**
SAL-C	**DH5α harboring PDMG4+PCAL**	**this study**
SAL-CO	**DH5α harboring PODMG4+POCAL**	**this study**
SAL-C-H149D	**DH5α harboring PDMG4+PCAL-H149D**	**this study**
SAL-C-H149S	**DH5α harboring PDMG4+PCAL-H149S**	**this study**
SAL-C-T68L	**DH5α harboring PDMG4+PCAL-T68L**	**this study**
SAL-H	**DH5α harboring PDMG4+PHAL**	**this study**
SAL-HO	**DH5α harboring PODMG4+POHAL**	**this study**
SAL-H-H149D	**DH5α harboring PDMG4+PHAL-H149D**	**this study**
SAL-H-H149S	**DH5α harboring PDMG4+PHAL-H149S**	**this study**
SAL-H-T68L	**DH5α harboring PDMG4+PHAL-T68L**	**this study**

311 Table S4. Plasmids used in this study. Related to Figure 1,2,3,5,6,7 and 8.

Plasmids	Charecteristics	Source
P0	**pACYC184 contains gfp and HrtR**	**this study**
P1	**pACYC184 contains HrtO, gfp and HrtR**	**this study**
P1-T68L	**pACYC184 contains gfp and HrtR-T68L**	**this study**
P1-V131L	**pACYC184 contains gfp and HrtR-V131L**	**this study**
P1-V131I	**pACYC184 contains gfp and HrtR-V131I**	**this study**
P1-H149D	**pACYC184 contains gfp and HrtR-H149D**	**this study**
P1-H149S	**pACYC184 contains gfp and HrtR-H149S**	**this study**
PSO	**pUC19 contains HrtR and HrtO-ineffective sgRNA**	**this study**
PSA	**pUC19 contains HrtR and HrtO-sgRNA-A**	**this study**
PSB	**pUC19 contains HrtR and HrtO-sgRNA-B**	**this study**
POSB	**pUC19 contains HrtR and sgRNA-B**	**this study**
PDMG1	**pACYC184 contains mkate2 and dcas9 (promoter:$_{J23113}$)**	**this study**
PDMG2	**pACYC184 contains mkate2 and dcas9 (promoter:$_{J23117}$)**	**this study**
PDMG3	**pACYC184 contains mkate2 and dcas9 (promoter:$_{J23114}$)**	**this study**
PDMG4	**pACYC184 contains mkate2 and dcas9 (promoter:$_{J23110}$)**	**this study**
PDMG5	**pACYC184 contains mkate2 and dcas9 (promoter:$_{J23100}$)**	**this study**
PODMG4	**PDMG4 deletes HrtO**	**this study**
PBH1	**pSIB contains sgRNA-1**	**this study**
PBH2	**pSIB contains sgRNA-2**	**this study**
PBH3	**pSIB contains sgRNA-3**	**this study**
POBH2	**pSIBH2 with the deletion of HrtO**	**this study**
PDMG4-1	**The promoter of mkate2 in PDMG4 was replaced with J23110**	**this study**
PDMG4-2	**The promoter of mkate2 in PDMG4 was replaced with J23101**	**this study**
PDMG4-3	**The promoter of mkate2 in PDMG4 was replaced with J23106**	**this study**
POBH2-AL	**POBH2 added *hemA*/*hemL***	**this study**
PSB-AL	**PSB added *hemA*/*hemL***	**this study**
PBH2-AL	**PBH2 added *hemA*/*hemL***	**this study**
PBH2ALT	**PBH2AL added tRNA-GLU**	**this study**
PBH2ALTG	**PBH2ALT added *rhtA* and *gdhA***	**this study**
PBH2ALTG-T68L	**PBH2ALTG with HrtR-T68L**	**this study**
PBH2ALTG-V131L	**PBH2ALTG with HrtR-V131L**	**this study**
PBH2ALTG-V131I	**PBH2ALTG with HrtR-V131I**	**this study**
PBH2ALTG-H149D	**PBH2ALTG with HrtR-H149D**	**this study**
PBH2ALTG-H149S	**PBH2ALTG with HrtR-H149S**	**this study**
PCAL	**replace with sgRNA targeting *hemC* on the basis of PBH2ALT**	**this study**
POCAL	**PCAL with the deletion of HrtO**	**this study**
PCAL-H149D	**PCAL with HrtR-H149D**	**this study**
PCAL-H149S	**PCAL with HrtR-H149S**	**this study**
PCAL-T68L	**PCAL with HrtR-T68L**	**this study**
PHAL	**replace with sgRNA targeting *hemH* on the basis of PBH2ALT**	**this study**
POHAL	**PHAL with the deletion of HrtO**	**this study**

PHAL-H149D	**PHAL with HrtR-H149D**	**this study**
PHAL-H149S	**PHAL with HrtR-H149S**	**this study**
PHAL-T68L	**PHAL with HrtR-T68L**	**this study**
PCHUA	**pcolAduet1 contains *chuA***	**this study**
p15b-WT	**p15b contains HrtR-WT**	**this study**
p15b-H149D	**p15b contains HrtR-H149D**	**this study**
p15b-H149S	**p15b contains HrtR-H149S**	**this study**
p15b-T68L	**p15b contains HrtR-T68L**	**this study**
p15b-V131L	**p15b contains HrtR-V131L**	**this study**
p15b-V131I	**p15b contains HrtR-V131I**	**this study**

References

Bayly, C.I., Cieplak, P., Cornell, W.D., and Kollman, P.A. (1993). A Well-Behaved Electrostatic Potential Based Method Using Charge Restraints for Deriving Atomic Charges - the Resp Model. J Phys Chem-Us *97*, 10269-10280.

Case, D.A., Cheatham, T.E., Darden, T., Gohlke, H., Luo, R., Merz, K.M., Onufriev, A., Simmerling, C., Wang, B., and Woods, R.J. (2005). The Amber biomolecular simulation programs. J Comput Chem *26*, 1668-1688.

Essmann, U., Perera, L., Berkowitz, M.L., Darden, T., Lee, H., and Pedersen, L.G. (1995). A Smooth Particle Mesh Ewald Method. J Chem Phys *103*, 8577-8593.

Gibson, D.G., Young, L., Chuang, R.Y., Venter, J.C., Hutchison, C.A., and Smith, H.O. (2009). Enzymatic assembly of DNA molecules up to several hundred kilobases. Nat Methods *6*, 343-U341.

Kang, Z., Wang, Y., Gu, P.F., Wang, Q., and Qi, Q.S. (2011). Engineering Escherichia coli for efficient production of 5-aminolevulinic acid from glucose. Metab Eng *13*, 492-498.

Kollman, P.A., Massova, I., Reyes, C., Kuhn, B., Huo, S.H., Chong, L., Lee, M., Lee, T., Duan, Y., Wang, W.*, et al.* (2000). Calculating structures and free energies of complex molecules: Combining molecular mechanics and continuum models. Accounts of chemical research *33*, 889-897.

Liu, N., Zhou, W.F., Guo, Y., Wang, J.M., Fu, W.T., Sun, H.Y., Liu, D., Duan, M.J., and Hou, T.J. (2018). Molecular Dynamics Simulations Revealed the Regulation of Ligands to the Interactions between Androgen Receptor and Its Coactivator. J Chem Inf Model *58*, 1652-1661.

Maier, J.A., Martinez, C., Kasavajhala, K., Wickstrom, L., Hauser, K.E., and Simmerling, C. (2015). ff14SB: Improving the Accuracy of Protein Side Chain and Backbone Parameters from ff99SB. Journal of chemical theory and computation *11*, 3696-3713.

Mazumder, D., and Case, D.A. (2007). AMBER Score in DOCK6: Application of molecular dynamics simulations and implicit solvent model (GB/SA) in protein-ligand docking. Abstr Pap Am Chem S *233*, 20-20.

Ryckaert J P , C.G., Berendsen H J C . (1976). Numerical integration of the cartesian equations of motion of a system with constraints: molecular dynamics of n-alkanes[J]. Journal of Computational Physics, 327-341.

Sawai, H., Yamanaka, M., Sugimoto, H., Shiro, Y., and Aono, S. (2012). Structural Basis for the Transcriptional Regulation of Heme Homeostasis in Lactococcus lactis. J Biol Chem *287*, 30755-30768.

Seminario, J.M. (1996). Calculation of intramolecular force fields from second-derivative tensors. Int J Quantum Chem *60*, 1271-1277.

Taverna, P., Rendahl, K., Jekic-McMullen, D., Shao, Y., Aardalen, K., Salangsang, F., Doyle, L., Moler, E., and Hibner, B. (2007). Tezacitabine enhances the DNA-directed effects of fluoropyrimidines in human colon cancer cells and tumor xenografts. Biochem Pharmacol *73*, 44-55.

Villarino, L., Splan, K.E., Reddem, E., Alonso-Cotchico, L., de Souza, C.G., Lledos, A., Marechal, J.D., Thunnissen, A.M.W.H., and Roelfes, G. (2018). An Artificial Heme Enzyme for Cyclopropanation Reactions. Angew Chem Int Edit *57*, 7785-7789.

Wang, J.M., Wolf, R.M., Caldwell, J.W., Kollman, P.A., and Case, D.A. (2004). Development and testing of a general amber force field. J Comput Chem *25*, 1157-1174.

383 Weiser, J., Shenkin, P.S., and Still, W.C. (1999). Approximate solvent-accessible
384 surface areas from tetrahedrally directed neighbor densities. Biopolymers *50*, 373-
385 380.

386